

Multi-wavelength view of an M2.2 Solar Flare on 26 November 2000

R. Chandra

Department of Physics, DSB Campus, Kumaun University, Nainital -263 001, India

V. K. Verma

Uttarakhand Space Application Center, Dehradun - 248 006, India

S. Rani

Department of Physics, DSB Campus, Kumaun University, Nainital - 263 001, India

R. A. Maurya

National Institute of Technology, Calicut - 673 601, India

Abstract

In this paper, we present a study of an M2.2 class solar flare of 26 November 2000 from NOAA AR 9236. The flare was well observed by various ground based observatories (ARIES, Learmonth's Solar Observatory) and space borne instruments (SOHO, HXRS, GOES) in time interval between 02:30 UT to 04:00 UT. The flare started with long arc-shape outer flare ribbon. Afterwards the main flare starts with two main ribbons. Initially the outer ribbons start to expand with an average speed ($\sim 20 \text{ km s}^{-1}$) and later it shows contraction. The flare was associated with partial halo coronal mass ejection (CMEs) which has average speed of 495 km s^{-1} . The SOHO/MDI observations show that the active region was in quadrupolar magnetic configuration. The flux cancellation was observed before the flare onset close to flare site. Our analysis indicate the flare was initiated by the magnetic breakout mechanism.

Keywords: Sun: solar flares - Sun: reconnections - Sun: coronal mass ejections

1. Introduction

Solar flare are large explosion in the Sun's atmosphere that can release as much as 6×10^{25} joules of energy (for review see Benz (2008)). Solar flares affect

*Corresponding author

Email address: rchandra.nt1@gmail.com (R. Chandra)

all layers of the solar atmosphere, heating plasma to tens of millions of Kelvin and accelerating electrons, protons (Gopalswamy et al., 2004; Chandra et al., 2013). They produce radiation across the whole electromagnetic spectrum i.e. from radio waves to gamma rays. Major goals of solar flare research is to determine the origin and evolution of the energetic electrons accelerated during impulsive phase of the solar flares. These particles are most directly observable through their gyro-synchrotron radiations at microwave (MW) frequencies and emission of hard X-ray (HXR) through collisional bremsstrahlung (Holman et al., 1984).

It is now widely accepted that solar flares are produced by the release of energy stored in the stressed magnetic field. Magnetic reconnection is mainly responsible for this energy release. Continuous flux emergence in the active region is one of the main indicator for the stressed magnetic field, whereas the flux cancellation can tell about the reconnection. The magnetic flux may already be twisted while emerging in the photosphere. The photospheric motion of magnetic polarities are the drivers of the free energy storage and the emerging flux would provide the trigger mechanism for the impulsive energy release. Therefore magnetic flux emergence and cancellation are very important to understand the causes of flare initiation.

The release energy during solar flares produces accelerated electrons and ions, which interact with the ambient solar atmosphere. High temporal resolution observations are very important to investigate the time evolution of solar flares. This allow us to study the different phases of flare evolution viz. impulsive, main and gradual phase. Therefore, analysis of multi-wavelength data with high spatial and temporal resolution is crucial for understanding the acceleration and propagation of particles during solar flares (for example see Aulanier et al. (2000); Galsgaard et al. (2000); Fletcher et al. (2001); Chandra et al. (2006, 2013) and references therein).

It is now established that flares and coronal mass ejections (CMEs) are predominantly magnetic explosions and they show rapid motion and heating that infer to be driven by magnetic energy locally contained in the magnetic field (Svestka et al., 1976; Sturrock, 1980). All CMEs and many flares exhibit outward mass motion, even though it is likely that part of the magnetic field must shrink (implode) in order that there be an overall decrease in magnetic energy in the region of the explosion (Hudson, 2000). The origins of CMEs were earlier investigated by Verma & Pande (1989) and Verma (1992, 2002) and suggested that the CME events are perhaps produced by some mechanism, in which the mass ejected by some solar flares or active prominences, gets connected with the open magnetic lines of CHs (coronal holes: source of high speed solar wind streams) and moves along them to appear as CMEs.

To explain the different observational features of solar flares and associated phenomena, the CSHKP model was proposed (Carmichael, 1964; Sturrock, 1966; Hirayama, 1974; Kopp & Pneuman, 1976). This model explains the filament eruptions, flare ribbon formation and their separation. The CSHKP model is two-dimensional. Recently Aulanier et al. (2013) and Janvier et al. (2013) extend the 2D CSHKP model into 3D using MHD simulations and compare

the numerical results with high resolution *Solar Dynamics Observatory (SDO)* observations. However, these models are not to explain the trigger mechanism of solar eruptions.

To understand the trigger mechanism of solar eruptions several models have been put forward. These models includes: Magnetic breakout (Antiochos et al., 1999), Tether cutting (Moore et al., 2001), kink instability (Török et al., 2004), ideal MHD instability (torus instability) (Forbes & Isenberg, 1991; Kliem & Török, 2006). However, it is still not settled which model initiates the solar eruptions. Therefore, to understand the solar eruptions trigger mechanism is still major problem in solar physics.

Here, we discuss about the “magnetic breakout” model, because it appears to be favorable mechanism for our studied event. According to this model, the eruption is triggered at the magnetic null-point high in the corona in a quadrupolar magnetic configuration. If the magnetic arcade starts to rise due to shear in magnetic field, its expansion results in the formation of a current sheet and reconnection at null-point. Due to the reconnection, the magnetic tension decreased continuously and as a result the eruption starts.

Several studies have been done on the observational evidence of magnetic breakout model (Aulanier et al. (2000); Mandrini et al. (2006); Joshi et al. (2007); Chandra et al. (2011); Aurass et al. (2011); Reeves et al. (2015); Chen et al. (2016) and references cited therein). Let us discuss these studies in brief. Aulanier et al. (2000) did the detailed analysis of Bastille day flare of 14 July, 1998 and concluded the eruption was due to the magnetic breakout. With the help of magnetic field extrapolations, they found the presence of a null point in the corona. Mandrini et al. (2006) studied the precursor phase of X17 flare on 28 October, 2003. They have reported a precursor event in $H\alpha$ and TRACE images in a large-scale quadrupolar reconnection and concluded that this precursor contributes to decrease magnetic tension and allows the filament to erupt in a way similar to breakout model. However, they showed that the magnetic reconnection occurs in Quasi-Separatrix Layers (QSLs) instead of null point. Chandra et al. (2011) also presented the evidence of magnetic breakout mechanism in the flare of 20 November, 2003 without the null-point topology. Joshi et al. (2007) and Aurass et al. (2011) shows the evidence of magnetic breakout on the basis of radio observations. Very recently Chen et al. (2016) presented the observations of imaging of magnetic breakout using the high resolution SDO data and found the breakout reconnection sets around 40 min before the main flare onset. From the above discussion on magnetic breakout mechanism, it is still not clear when and where the eruption is triggered in this mechanism. Hence, it needs further investigation.

Therefore to shed light on the above discussed problems, in this present paper, we have investigated an M2.2 solar flare and CMEs observed on 26 November, 2000 from NOAA AR 9236 in view of multi-wavelength observations. In section 2, we mentioned about observational data sources and an overview of active region. The results are presented in Section 3 and conclusion is given in section 4.

2. Observations and overview of the active region NOAA 9236

The active region, NOAA AR 9236 was one of the most flare productive active region in the peak phase of solar cycle 23. The active region appeared in the east limb on 18 November, 2000 as β magnetic configuration and went over the west limb on 30 November, 2000. The magnetic configuration of active region becomes $\beta\gamma$ on 23 November, 2000. During the disk passage the active region produced 40 C-class, 06 M-class, 10 X-class GOES X-ray flares. Many flares from this active region were studied by several authors (Nitta & Hudson, 2001; Wang et al., 2002; Moon et al., 2003; Takasaki et al., 2004). In these studies, it was reported that the active region was characterized by continuous magnetic flux emergence in the penumbral area sunspot. According to Wang et al. (2002), the flux emerged in the active region between 23 to 25 November, 2000. Afterwards the flux emergence stops.

On 2000 November 26, we observed an M2.2 class GOES flare /optical class 1F flare in $H\alpha$ from ARIES, Nainital in this active region. The active region was located on solar disk at N22W34 on that day. The flare impulsive phase starts around 02:47 UT, peaked at 03:08 UT, and ended around 03:20 UT.

In order to know the magnetic causes of the flare, we have presented the magnetic filed images before the flare onset in Figure 1. In the figure the top image shows the extended view of active region. The active region is in quadrupolar magnetic configuration. The negative/positive polarities of the quadrupole is shown by N1N2/P1P2 and enclosed by white and black contours respectively. The enlarged view of the active region shown by square in the top image is shown in the middle and bottom panel of the figure. We have circled the area of flare location. Looking at these circled regions, we noticed the significant flux cancellation before the onset of M2.2 class flare.

The observational data used in this study is taken from the following instruments:

- **$H\alpha$ Data:** For the current study we used the $H\alpha$ data observed from ARIES (formerly State Observatory), Nainital, India with 15 cm f/15 Coudé-refractor telescope. The telescope was equipped with high speed CCD camera developed for observations of solar flares, which is capable to record flare image at time interval of 25 ms. Details of the CCD camera system is described by Verma (1999). The resolution of images are 0.65 arcsec. The cadence of images during the observations was from one to ten sec during the flare observation.
- **X-ray and Radio Data:** To understand the thermal and non-thermal nature of the flare, we use the X-ray data from the Czech-made Hard X-Ray Spectrometer (HXRS) instrument on board the Multispectral Thermal Imager (MTI) satellite (Fárník et al., 2001). In addition of these data, we have used the radio data of different frequencies observed from Learmonth Solar Observatory.
- **SOHO/MDI and SOHO/EIT Data:** In order to study the magnetic complexity of the active region, we have used the data from Michelson

Doppler Imager (MDI) (Scherrer et al., 1995) onboard Solar and Heliospheric Observatory (SOHO) satellite. The cadence and the pixel size of the images are 96 min and 1.98 arcsec respectively. We have also used the SOHO/EIT Fe XII (195 Å) data (Delaboudinière et al., 1995). The cadence of EIT data was 12 min, and the pixel resolution was 2.5 arcsec.

- **LASCO CME Data:** For the associated CME with the studied flare, we used the data from Large Angle Spectroscopic Coronagraph (LASCO; Brueckner et al. (1995)) C2 data.

3. Analysis and Results

To understand the multi-wavelength spatial and temporal characteristics of the flare, in this section, the evolution of the flare observed in H α , radio, X-ray and EUV wavebands is presented.

3.1. Spatial Evolutions

Figure 2 shows the evolution of the M2.2/1F class flare in H α . One difference between our studied event here and other previous flare from this active region is that, most of the previous observed flares were initiated by filament eruption. In contrary to that the flare of 26 November, 2000 was not associated with any filament eruption. However, this flare looks homologous to the other flares of this active region. Similar to other homologous flare, this flare was also associated with partial halo CME. The description about the associated CME is discussed in subsection 3.3.

The flare was initiated with arc-shaped ribbon R1 around 02:48 UT. The ribbon R1 has two parts eastern (R1') and western (R1). The eastern fainter ribbon R1' faded quickly. We track the evolution of western ribbon R1 and found, initially the north portion of ribbon was moving towards west with a speed of $\sim 20 \text{ km s}^{-1}$. As the time progress the same part of the ribbon shows contraction. The north part of the ribbon R1 faded; while as the south part was bright till the end of the main flare. This ribbon was located in the positive polarity region (see figure 3). Such arc-shaped type ribbons were observed in all the flares produced by this active region (Wang et al., 2002; Takasaki et al., 2004). Wang et al. (2002) interpret these arc-shaped ribbons as a results of the interaction between erupting flux rope and the overlaying loops. Wang (2005) also found the expansion-to-contraction motion in the outer ribbon of 25 November, 2000 flare event from the same active region. As proposed by Wang (2005), this contraction motion can be interpreted as a result of the falling back of part of erupting flux rope. Such arc-shaped ribbons was also reported in Chandra et al. (2009).

The first appearance of arc-shaped ribbon R1 indicates weak reconnection first and as a result of this the ribbon R1 appears. After the weak reconnection, it might weakend the magnetic tension. Afterwards the main flare occur. This could be a signature of the magnetic breakout model as discussed in the introduction section. For the magnetic breakout trigger mechanism, the quadrupolar

configuration is a necessary condition. If we look at our active region, it has also quadrupolar structure (see figure 1).

According to magnetic breakout model proposed by Antiochos et al. (1999), the reconnection start to occur above the erupting arcade and not much energy is released during this reconnection. The reason is that most of the free energy is stored in the low laying arcade. Due to the weak reconnection, we might observed the arc-shaped outer ribbon in one of the positive polarity ‘P2’ of quadrupolar magnetic configuration (see figure 1, upper panel). The appearance of outer ribbon before the main flare is an important implication of the breakout model. Hence, we believe that the quadrupolar magnetic configuration together with the first appearances of arc-shaped ribbon R1 strengthen our idea that the flare was triggered by magnetic breakout mechanism.

Quickly after the appearance of arc-shaped ribbon R1, main flare ribbons R2 and R3 start to brighten. The main flare ribbons can be seen up to 03:30 UT. As the time progresses these main flare ribbons show the sign of separation as expected in CSHKP flare model. To locate the location of polarity of flare ribbons in Figure 3 (top, left panel), the contours of flare ribbons are plotted over magnetogram. The overplot shows that the main flare ribbon R2 and R3 are located in the positive and negative polarities respectively.

Figure 3 also presented (top right, bottom (left,right)) the SOHO/EIT 195 Å images at flare onset and during the flare maximum phase. Figure 3 (bottom, left) shows the SOHO/EIT image overlaid by MDI magnetic field contours. The black and white contours represent the negative and positive polarity respectively. In the bottom, right image, we can see the loops joining the ribbon R1 R2 and R2 R3. These loops indicate the connectivity after the flare. Evolution of main flare ribbons R1 and R2 shows several kernels inside the ribbons. The temporal evolution of some of the selected kernels is presented in next subsection.

3.2. Temporal Evolutions

To study the temporal association of observed flare among different wavelengths, in this section, we have presented the intensity evolution of flare as a function of time observed in $H\alpha$, soft X-rays, hard X-rays, and radio wavelengths. As mentioned in previous subsection, during the evolution of the flare in $H\alpha$, we can see several kernels. we have selected three kernels, as shown in Figure 2 at 3:11:25 UT. We name them K1, K2 and K3 respectively. For the computation of flare kernel intensity, we have created a box of 10×10 pixels around the kernels and calculate the average intensity inside it. Afterwards the average intensity is normalized by the background intensity. For the background intensity we have selected a box of 100×100 pixels in the quiet region. Among the selected kernels K1, and K3 are strong. Therefore for the temporal evolution, we have plotted only the kernel K1 and K3.

In the panel I, II and III of Figure 4, we have plotted the GOES X-ray at two wavelengths, GOES X-ray time derivative and HXRS hard X-rays, data respectively. The $H\alpha$ kernels are displayed in IV, V of the figure, whileas VI panel presents the radio observations at frequencies 1415 MHz, 2695 MHz, 4995 MHz,

8800 MHz and 15400 observed from Learmonth Solar Observatory, Learmonth, Australia.

The impulsive phase of flare (between 02:50 to 02:58 UT) was observed by HXRS at different energy channels. The impulsive phase of X-ray peaks around 02:54 UT. Unfortunately, the HXRS X-ray observations was not available during the peak phase of flare. According to Neupert effect the time derivative of soft X-ray should correlate with the Hard X-rays. Therefore, to fill the gap of HXRS observation, We have taken GOES time derivative as a proxy of Hard X-rays. The time derivative of the GOES X-rays is shown in figure 4 (second panel). We have noticed the GOES time derivative is peaked earlier (~ 4 min) then the GOES soft X-ray and $H\alpha$. This suggests that the acceleration of non-thermal electrons was involved in the heating of lower chromosphere.

Looking at the radio profiles, we noticed two peak: the first peak was associated with HXRS peaks, whereas the second peak was associated with main flare phase observed in $H\alpha$ and GOES SXR. The temporal correlation between the first radio peaks and HXR peaks indicate that the same population of electrons are responsible for the HXR and radio emissions.

If we compare the onset of X-rays, radio flux and the appearance of flare ribbon R1. They are temporally associated. This indicate that the before the main phase of flare, there is a weak reconnection, which triggers the main flare. This is the evidence of flare trigger due to magnetic breakout mechanism. The description about the ribbon R1 is discussed in subsection 3.1.

3.3. CME Observations

The solar flare observed on 2000 November 26 at 02:27 UT was accompanied by partial CME (width ~ 259 deg) as observed by the LASCO instrument. The CME appear first in LASCO C2 field-of-view at 03:30 UT in the north-west direction. The evolution of LASCO C2 CME is displayed in Figure 5. The linear velocity of CMEs is 495 km s^{-1} . The acceleration corresponding to CMEs was -22.9 ms^{-2} .

4. Conclusions

In this study, we have presented the high cadence CCD observations of an M2.2 class solar flare in $H\alpha$ emissions on 2000 November, 26 from NOAA AR 9236. The ground based $H\alpha$ was combined with radio observations and with various space borne instruments (SOHO, HXRS, GOES).

The flare started with long arc-shape outer R1 ribbons. Afterwards the main flare starts with two ribbons. Initially the outer ribbons start to expand with average speed of 20 km s^{-1} and lateron it shows contraction. The first appearance of outer flare ribbons and quadrupolar magnetic configuration of active region shows that the flare was initiated by the magnetic breakout mechanism (Antiochos et al., 1999). The appearance of X-ray and radio emission flux before the main flare also confirm that the flare is triggered by magnetic breakout mechanism.

The SOHO/MDI observations shows emergence of positive and negative magnetic polarities around the main positive polarity, which might makes this active region more flare productive. The cancellation of magnetic flux close to the flare site before the studied M2.2 class flare could provide the evidence that that flux cancellation is responsible for the flare.

Acknowledgments

We thank the anonymous referee for the valuable comments and suggestions. The authors are thankful to LASCO/SOHO, HXRS and Learmonth Solar Observatory, Learmonth, Australia whose data are used in the present investigation. The CME catalog is generated and maintained at the CDAW Data Center by NASA and The Catholic University of America in cooperation with the Naval Research Laboratory. SOHO is a project of international cooperation between ESA and NASA.

References

- Antiochos, S. K., DeVore, C. R., & Klimchuk, J. A. (1999). *ApJ*, *510*, 485–93.
- Aulanier, G., DeLuca, E. E., Antiochos, S. K., McMullen, R. A., & Golub, L. (2000). *ApJ*, *540*, 1126–42.
- Aulanier, G., Démoulin, P., Schrijver, C. J., Janvier, M., Pariat, E., & Schmieder, B. (2013). *Astron. Astrophys.*, *549*, A66.
- Aurass, H., Mann, G., Zlobec, P., & Karlický, M. (2011). *ApJ*, *730*, 57.
- Benz, A. O. (2008). *Living Reviews in Solar Physics*, *5*.
- Brueckner, G. E., Howard, R. A., Koomen, M. J., Korendyke, C. M., Michels, D. J., Moses, J. D., Socker, D. G., Dere, K. P., Lamy, P. L., Llebaria, A., Bout, M. V., Schwenn, R., Simnett, G. M., Bedford, D. K., & Eyles, C. J. (1995). *Sol. Phys.*, *162*, 357–402.
- Carmichael, H. (1964). In W. N. Hess (Ed.), *The Physics of Solar Flares* (p. 451).
- Chandra, R., Gopalswamy, N., Mäkelä, P., Xie, H., Yashiro, S., Akiyama, S., Uddin, W., Srivastava, A. K., Joshi, N. C., Jain, R., Awasthi, A. K., Manoharan, P. K., Mahalakshmi, K., Dwivedi, V. C., Choudhary, D. P., & Nitta, N. V. (2013). *Advances in Space Research*, *52*, 2102–11.
- Chandra, R., Jain, R., Uddin, W., Yoshimura, K., Kosugi, T., Sakao, T., Joshi, A., & Deshpande, M. R. (2006). *Sol. Phys.*, *239*, 239–56.
- Chandra, R., Schmieder, B., Aulanier, G., & Malherbe, J. M. (2009). *Sol. Phys.*, *258*, 53–67.

- Chandra, R., Schmieder, B., Mandrini, C., Démoulin, P., Pariat, E., Török, T., & Uddin, W. (2011). *Sol. Phys.*, *269*, 83–104.
- Chen, Y., Du, G., Zhao, D., Wu, Z., Liu, W., Wang, B., Ruan, G., Feng, S., & Song, H. (2016). *ApJL*, *820*, L37.
- Delaboudinière, J., Artzner, G. E., Brunaud, J., Gabriel, A. H., Hochedez, J. F., Millier, F., Song, X. Y., Au, B., Dere, K. P., Howard, R. A., Kreplin, R., Michels, D. J., Moses, J. D., Defise, J. M., Jamar, C., Rochus, P., Chauvineau, J. P., Marioge, J. P., Catura, R. C., Lemen, J. R., Shing, L., Stern, R. A., Gurman, J. B., Neupert, W. M., Maucherat, A., Clette, F., Cugnon, P., & van Dessel, E. L. (1995). *Sol. Phys.*, *162*, 291–312.
- Fárník, F., Garcia, H., & Karlický, M. (2001). *Sol. Phys.*, *201*, 357–72.
- Fletcher, L., López Fuentes, M. C., Mandrini, C. H., Schmieder, B., Démoulin, P., Mason, H. E., Young, P. R., & Nitta, N. (2001). *Sol. Phys.*, *203*, 255–87.
- Forbes, T. G., & Isenberg, P. A. (1991). A catastrophe mechanism for coronal mass ejections. *ApJ*, *373*, 294–307.
- Galsgaard, K., Parnell, C. E., & Blaizot, J. (2000). *Astron. Astrophys.*, *362*, 395–405.
- Gopalswamy, N., Yashiro, S., Krucker, S., Stenborg, G., & Howard, R. A. (2004). *Journal of Geophysical Research (Space Physics)*, *109*, A12105.
- Hirayama, T. (1974). *Sol. Phys.*, *34*, 323–38.
- Holman, G. D., Kundu, M. R., & Dennis, B. R. (1984). *ApJ*, *276*, 761–5.
- Hudson, H. S. (2000). *ApJL*, *531*, L75–7.
- Janvier, M., Aulanier, G., Pariat, E., & Démoulin, P. (2013). *Astron. Astrophys.*, *555*, A77.
- Joshi, B., Manoharan, P. K., Veronig, A. M., Pant, P., & Pandey, K. (2007). *Sol. Phys.*, *242*, 143–58.
- Kliem, B., & Török, T. (2006). Torus Instability. *Physical Review Letters*, *96*, 255002.
- Kopp, R. A., & Pneuman, G. W. (1976). *Sol. Phys.*, *50*, 85–98.
- Mandrini, C. H., Demoulin, P., Schmieder, B., Deluca, E. E., Pariat, E., & Uddin, W. (2006). *Sol. Phys.*, *238*, 293–312.
- Moon, Y.-J., Chae, J., Wang, H., & Park, Y. D. (2003). *Advances in Space Research*, *32*, 1953–8.
- Moore, R. L., Sterling, A. C., Hudson, H. S., & Lemen, J. R. (2001). *ApJ*, *552*, 833–48.

- Nitta, N. V., & Hudson, H. S. (2001). *GRL*, *28*, 3801–4.
- Reeves, K. K., McCauley, P. I., & Tian, H. (2015). *ApJ*, *807*, 7.
- Scherrer, P. H., Bogart, R. S., Bush, R. I., Hoeksema, J. T., Kosovichev, A. G., Schou, J., Rosenberg, W., Springer, L., Tarbell, T. D., Title, A., Wolfson, C. J., Zayer, I., & MDI Engineering Team (1995). *Sol. Phys.*, *162*, 129–88.
- Sturrock, P. A. (1966). *Nature*, *211*, 695–7.
- Sturrock, P. A. (1980). In P. A. Sturrock (Ed.), *Skylab Solar Workshop II* (pp. 411–49).
- Svestka, Z., de Jager, C., Obayashi, T., Annis, M., & de Feiter, L. D. (1976). *Sol. Phys.*, *47*, 1–432.
- Takasaki, H., Asai, A., Kiyohara, J., Shimojo, M., Terasawa, T., Takei, Y., & Shibata, K. (2004). *ApJ*, *613*, 592–9.
- Török, T., Kliem, B., & Titov, V. S. (2004). *Astron. Astrophys.*, *413*, L27–30.
- Verma, V. (1999). In T. R. Rimmele, K. S. Balasubramaniam, & R. R. Radick (Eds.), *High Resolution Solar Physics: Theory, Observations, and Techniques* (p. 288). volume 183 of *Astronomical Society of the Pacific Conference Series*.
- Verma, V. K. (1992). *Indian Journal of Radio and Space Physics*, *21*, 64–9.
- Verma, V. K. (2002). In P. C. H. Martens, & D. Cauffman (Eds.), *Multi-Wavelength Observations of Coronal Structure and Dynamics* (p. 319).
- Verma, V. K., & Pande, M. C. (1989). In B. M. Haisch, & M. Rodonò (Eds.), *Solar and Stellar Flares. Poster Papers* (pp. 239–42). volume 104.
- Wang, H. (2005). Properties of Remote Flare Ribbons Associated with Coronal Mass Ejections. *ApJ*, *618*, 1012–9. doi:10.1086/426104.
- Wang, H., Gallagher, P., Yurchyshyn, V., Yang, G., & Goode, P. R. (2002). *ApJ*, *569*, 1026–31.

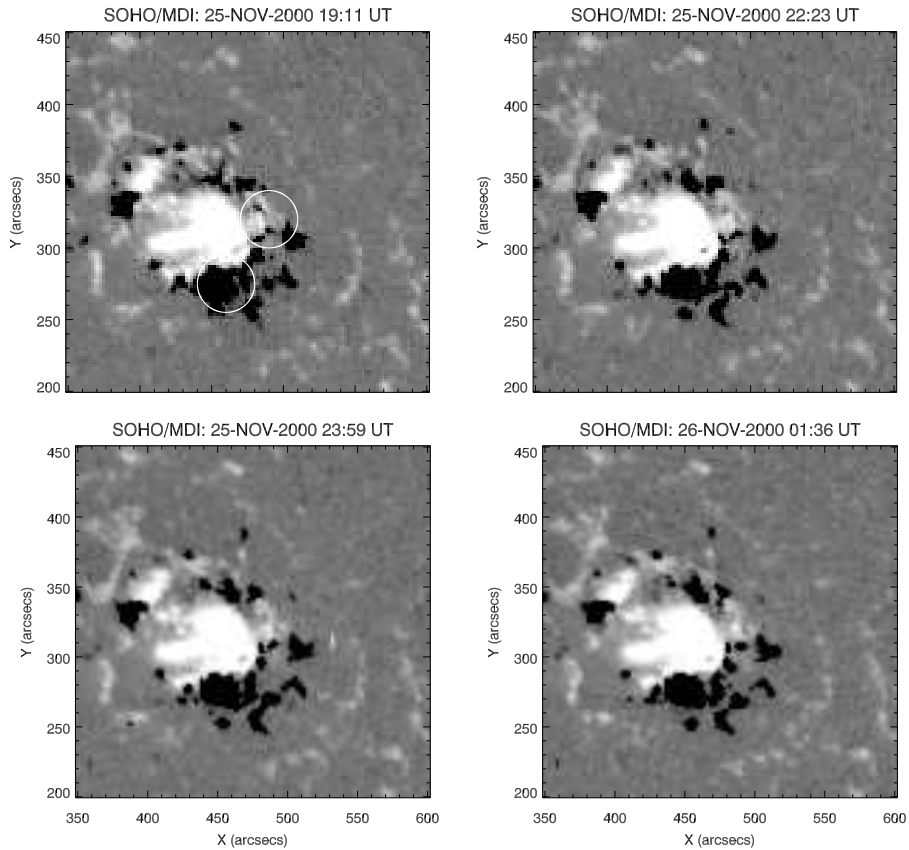
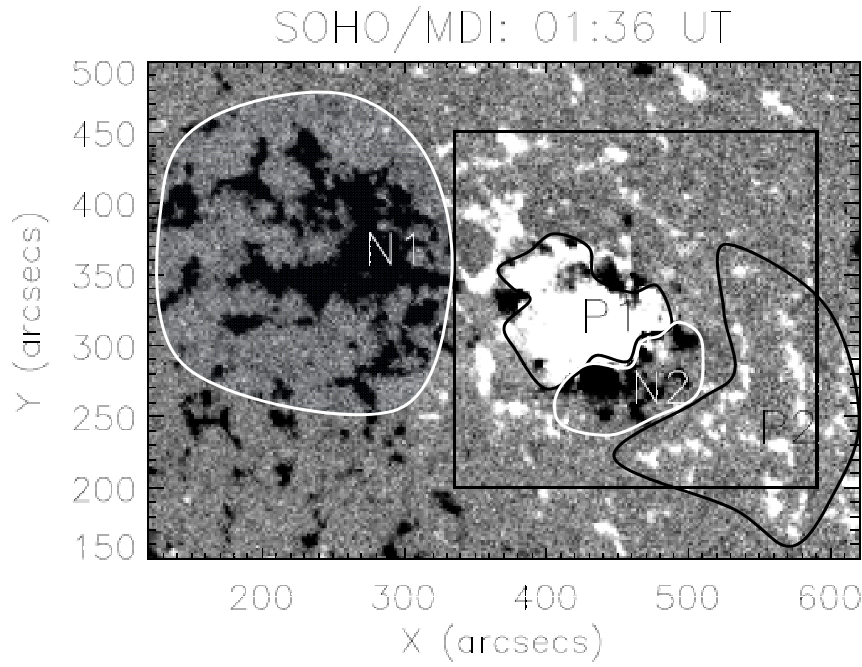


Figure 1: Top: Full view of active region, The different quadrupole negative/positive polarities are represented by N1,N2/P1,P2 respectively. The square in the figure represents the field-of-view enlarged in middle and bottom panels. Bottom and bottom panel: Evolution of SOHO/MDI line-of-sight magnetic field before the flare onset. The circles in the first image refers to the location, where magnetic flux cancellation occurs.

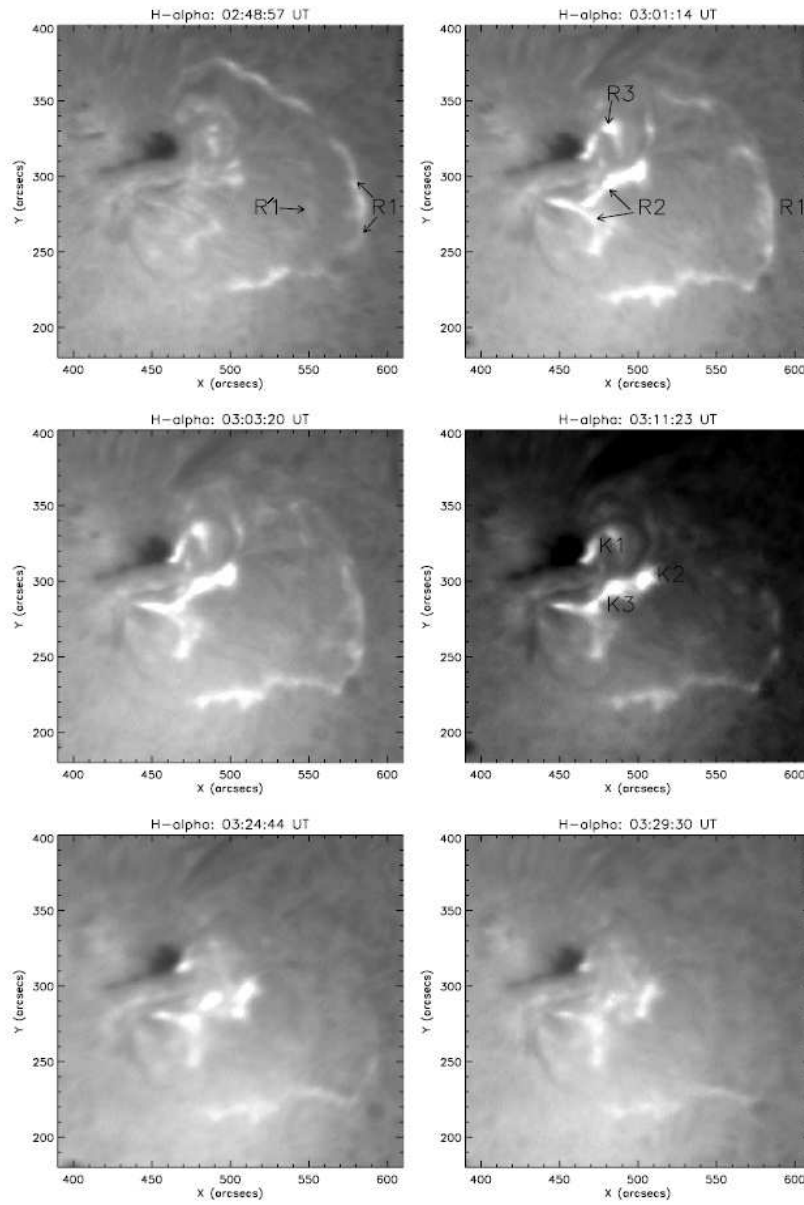


Figure 2: Evolution of flare in $H\alpha$ on 26 November, 2000. The locations of different ribbons and kernels are marked by R1, R1', R2, R3 and K1, K2, K3 respectively.

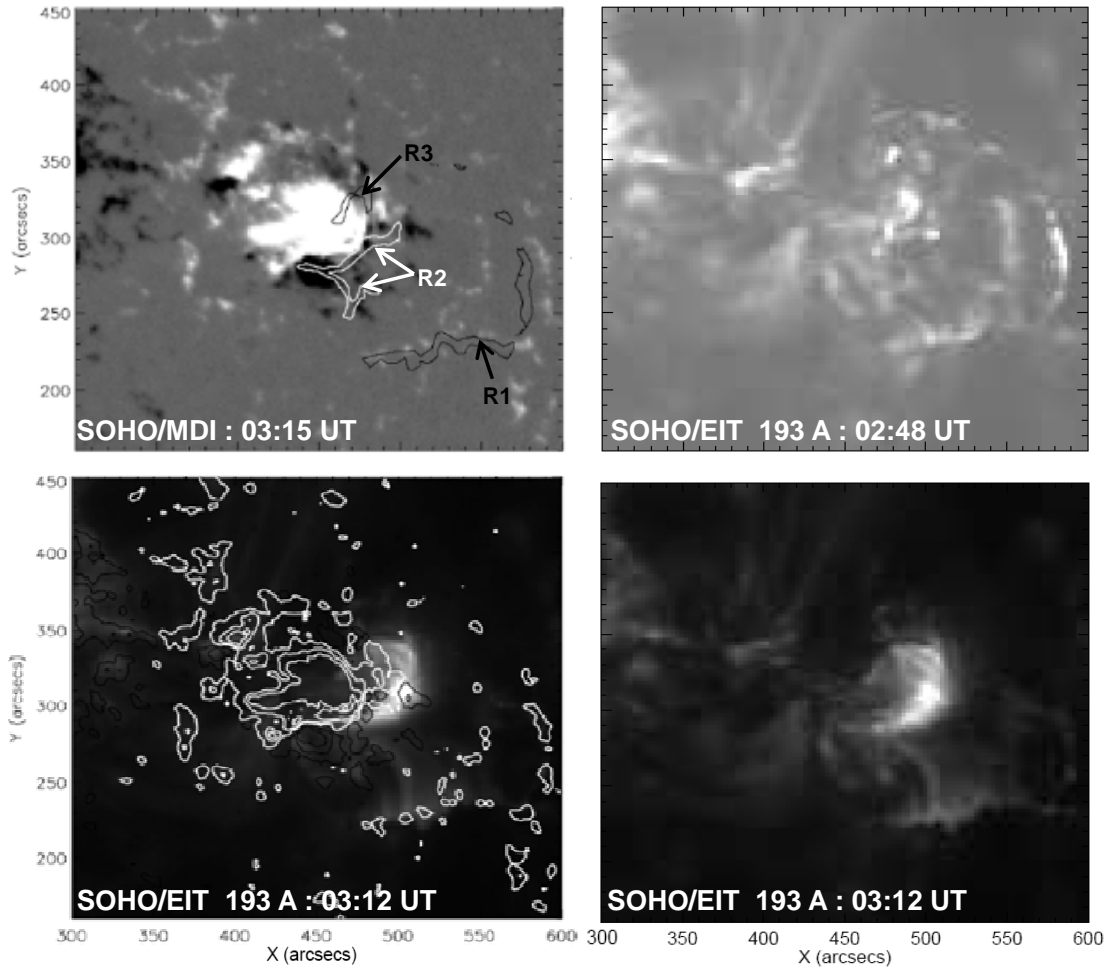


Figure 3: Location of H α ribbons on MDI magnetic field(top, left), SOHO/EIT 193 Å image at flare onset (top, right), SOHO/EIT 193 Å image overlaid by MDI contours (bottom, left), and peak phase of flare in SOHO/EIT 193 Å (bottom, right).

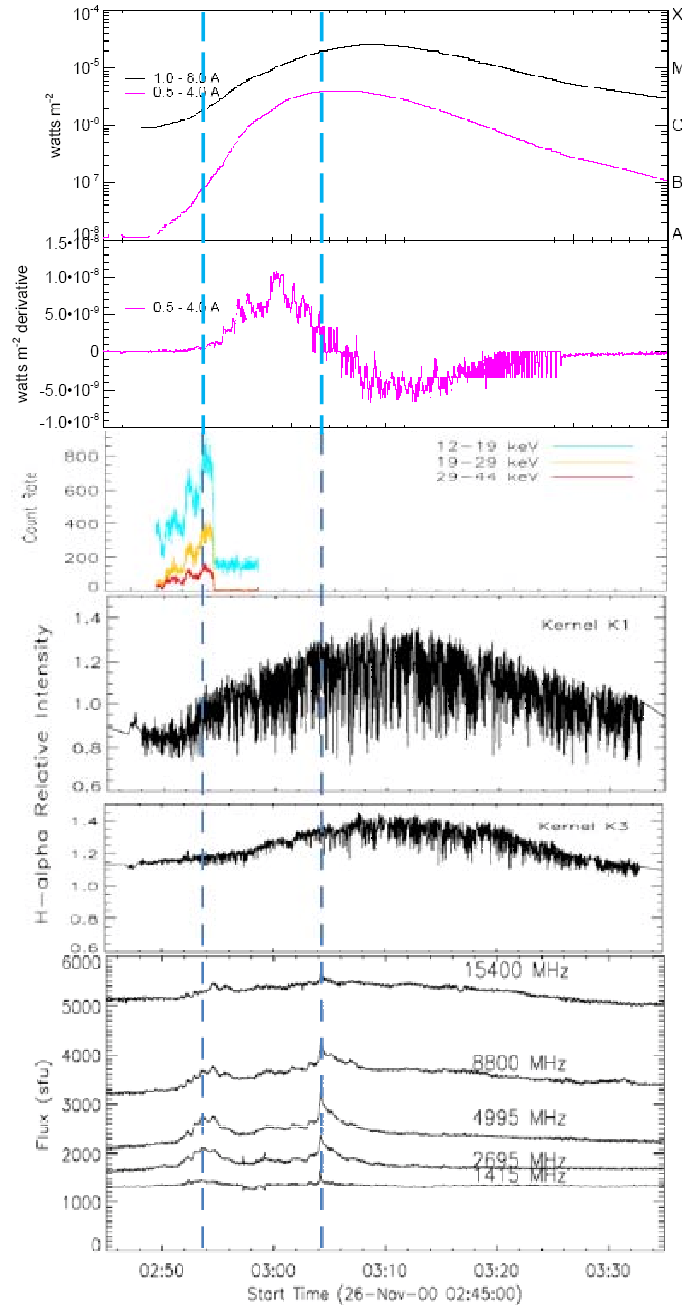


Figure 4: Temporal evolution of flare in X-rays, GOES time derivative, H α (flare kernels), and radio at different frequencies.

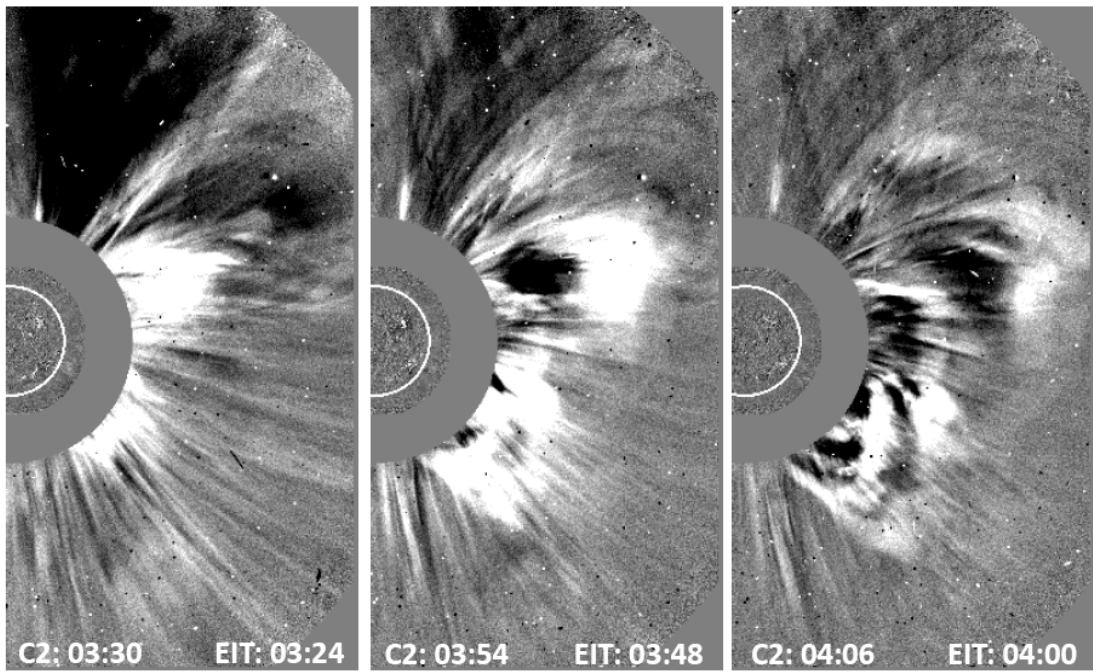


Figure 5: Evolution of associated CME observed by LASCO C2 on 26 November, 2000.